OPEN ACCESS
Journal of Multidisciplinary Applied Natural Science Vol. xx No. xx (xxxx) https://doi.org/10.47352/jmans.2774-3047.445
Check for updates
Research Article

Shrimp Shell-Based Solid-State Fermentation Promotes Dual Antibacterial and Cytotoxic Metabolite in *Kocuria palustris* 19C38A1

Widyastuti Widyastuti*, Fendi Setiawan, Ety Apriliana, Wawan A. Setiawan, and Peni Ahmadi

Received : December 11, 2025	Revised : March 5, 2026	Accepted : April 29, 2026	Online : June 25, 2026

Abstract
The growing impact of antimicrobial resistance (AMR) and cancer highlights the need to develop new and more effective therapeutic agents. Here, we explore a solid-state fermentation (SSF) strategy using shrimp-shell waste to stimulate secondary metabolite of marine *Kocuria palustris* 19C38A1. Bioautography-guided screening revealed that polar components of the extract (C38FA) showed antibacterial activity against multidrug-resistant *Staphylococcus aureus* (MIC = 250 µg/mL), The same fraction demonstrated pronounced cytotoxicity, inhibiting cell viability of A549 and HeLa cancer cells by 89% and 98%, respectively, at 100 µg mL^{-1} concentration, while showing weaker activity toward MCF-7 cells. Dereplication analysis using LC–MS/MS has annotated six putative metabolites such as terpendole B (**1**), *p*-hydroxyphenyl-acetylglutamic acid (**2**), istamycin C1 (**3**), lankacidin C (**4**), anthelmycin (**5**), and octacosa-hexaenoic acid (**6**) with mass accuracies within ±0.3 ppm. Notably, four of these compounds have well established antibacterial or cytotoxic properties, consistent with the dual *in vitro* bioactivity observed. ADME predictions suggested that compounds **1** and **2** are the most promising drug-like candidates, showing high gastrointestinal absorption and low cytochrome P450 liability. Furthermore, computational target prediction indicated potential interactions with proteases, kinases, oxidoreductases, and EGFR associated pathways, further hinting at their dual activity multifunctionality. Molecular docking suggested that compound **1** binds to FtsZ and EGFR, with predicted binding energies of -6.89 and -9.03 kcal/mol, respectively. Collectively, this work suggests that shrimp-shell waste can serve as a sustainable biogenic elicitor that induces marine actinobacteria to produce metabolites with dual pharmacological activities under SSF. These findings highlight a sustainable method for discovering potential dual activity antibacterial and anticancer bioactive compounds with therapeutic potential.

Keywords: antibacterial, cytotoxicity, *Kocuria palustris*, marine actinobacteria, shrimp shell, solid-state fermentation, waste valorization

1. INTRODUCTION

Worldwide demand for new antimicrobial agents is intensifying as multidrug-resistant bacterial pathogens become increasingly widespread [1]. Moreover, cancer remains one of the world's leading causes of morbidity and mortality, badly in need of new chemotherapeutic options [2]. These two crises increasingly intersect, as infections are a major cause of mortality in immuno-compromised cancer patients, creating an urgent need for therapeutic agents that can simultaneously address microbial infection and malignant disease [3]. Concurrent antibacterial and cytotoxic activities suggest clinical promise, not only for combating antimicrobial resistance but also for advancing dual -purpose therapeutics targeting infection-associated cancers and conditions of immune compromise [4]. Marine actinobacteria living in association with invertebrate hosts experience continual pressure from competitors for both space and nutrients, driving the production of secondary metabolites that serve defensive or signaling roles [5][6]. In this study, we define dual bioactivity as the capacity of a single microbial metabolite to exert both antibacterial and cytotoxic effects.

Dual bioactivity activities are common among these bioactive compounds of interest, increasing their suitability in future drug discovery [7][8]. Compounds such as anthracyclines, enediynes, and some macrolides have long been recognized for their antimicrobial origins and later were repurposed as anticancer agents owing to their ability to intercalate DNA or generate reactive oxygen species (ROS) [9][10]. Recently, marine-derived such as *Streptomyces*, *Salinispora*, and *Micromonospora* species have provided structurally unique secondary metabolites, including alkaloids, polyketides, and nonribosomal peptides, which

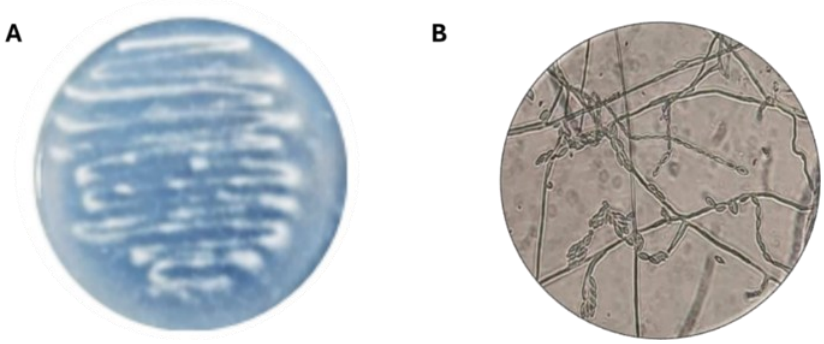

Figure 1. Isolate of 19C38A1 (a) in colloidal chitin agar media after 7 days and (b) light microscopy analysis 400 ×M.

exhibit growth-inhibitory effects against bacterial pathogens and tumor cell lines [11][12]. Yet, *Kocuria palustris*, which is found in association with marine organisms, is not well understood and has been studied very little so far [13]. While largely uncharacterized, such rare species often harbor silent biosynthetic gene clusters that, when appropriately triggered, can produce structurally unique and pharmacologically active metabolites [14].

Despite the recognized potential of marine actinobacteria, a critical gap remains most studies examine antibacterial or anticancer activities in isolation, while little is known about how cultivation strategies can be leveraged to induce dual bioactivity in underexplored marine species [15]. Consequently, advances in fermentation approaches have become central to unlocking their full biosynthetic and pharmacological potential [16]. Solid state fermentation (SSF) has recently received much attention due to its cost-effective and eco-friendly advantages for producing bioactive compounds [17][18]. Despite submerged fermentation (SmF), SSF could mimics the natural growth conditions for many microorganisms, leading to increased a broader range of unique metabolites [19]. Waste from seafood processing, such as shrimp shell waste, serves as especially valuable substrates for SSF. Shrimp shell are rich in chitin, proteins, and minerals that not only serve as a good nutrient source for microbial growth but also act as biogenic elicitors that stimulate secondary-metabolite biosynthesis and enhance bioactivity [20][21].

The use of shrimp-shell waste transforms an abundant environmental by-product into a value-added biotechnological resource, aligning natural-product discovery with circular-economy and sustainability principles [22]. Accordingly, shrimp-shell-based SSF provides an eco-conscious platform for generating bioactive metabolites from marine-derived actinobacteria with pharmaceutical relevance. In this landscape, marine-derived actinobacteria continue to represent a compelling frontier for natural products discovery. Metabolites exhibiting both antibacterial and cytotoxic activities offer promising avenues for identifying novel chemical scaffolds with relevance to infectious disease and oncology alike. Furthermore, integrating innovative cultivation approaches such as SSF using shrimp shell waste broadens the prospects for sustainable drug discovery. Here, we profile and evaluate the secondary metabolites of marine actinobacteria *Kocuria palustris* 19C38A1, underscoring their dual potential as antibacterial and cytotoxic agents.

2. MATERIALS AND METHODS

2.1. Isolates of Actinomycetes

The actinomycetes with code 19C38A1 were previously collected from marine invertebrates from Oluhuta, Tomini Bay, Gorontalo in 2019. The isolates were maintained on coloidal chitin agar media (consisting of 1 g of colloidal chitin, 2 g of nutrient agar, and 100 mL of artificial sea water) [17].

2.2. Morphological Analysis

Morphological characteristics of the isolate was performed using the coverslip insertion method at a 45° angle [23]. Briefly, sterile glass coverslips were

inserted diagonally into the solid medium so that one edge was embedded in the agar and the other protruded above the surface. The isolates were inoculated at the base of the coverslip, allowing mycelial growth and sporulation to extend onto the glass surface during incubation at 28 °C for 7 days. After incubation, the coverslips were carefully removed, placed on clean glass slides, and observed under a compound microscope (100–400×M) using brightfield and phase-contrast optics. Morphological features, including the development of substrate and aerial mycelia, spore chain arrangement, spore shape were recorded for taxonomic characterization.

2.3. Solid State Fermentation

Fresh shrimp shell waste were washed thoroughly, chopped into small pieces, kept moist, and sterilized by autoclaving at 121 °C for 20 min. The inoculum was prepared by growing the isolate in colloidal-chitin broth at 28 °C with shaking until active growth was achieved. Approximately 10%v/w inoculum was added to 150 g of moist, autoclaved shrimp shell in 2 L flasks, which were incubated statically at 28 °C for 14 days. At the end of fermentation, the substrate was extracted with ethyl acetate (EtOAc) concentrated under reduced pressure, and the crude extracts stored at −20 °C for antibacterial and cytotoxic assays.

2.4. Thin Layer Chromatgoraphy (TLC) Analysis

As the preliminary compound identification, the TLC was used using Silica gel GF254 as stationary phase, the mixture of *n*-hexane:EtOAc with ratio of 1:1, as mobile phase. The identification was performed under UV lamp at 254 and 366 nm and several reagent such as cerium sulphate and Dragendorff's reagent.

2.5. Antibacterial Activity

The evaluation of antibacterial actvity was performed following the method of Setiawan et al. [24]. To silica gel TLC plates, 10 µL of crude extracts (20,000 ppm) was applied and developed in *n*-hexane:EtOAc (1:1), plates were air-dried and heat-dried at 60 °C for 10 min to remove residual solvent. Preparation of a fresh overnight culture of the test bacterium, dilute to 1×10^6 CFU/mL in sterile triptyc soy broth (TSB). Melt and cool sterile overlay agar (0.8% agar in suitable growth medium) to 45 °C; mix with the bacterial suspension to give a final volume sufficient for one plate (typically 15 mL overlay per 10×10 cm plate). Pour the inoculated molten overlay evenly over each TLC plate and allow solidification under sterile conditions. The overlaid plates are incubated upright at 37 °C for 18 h. After incubation, add 1 mL of 0.02% w/v resazurin solution evenly across each plate using a sterile glass spreader or by gentle spraying and incubated it for 15 min at room temperature to allow color development. Areas where bacterial metabolism is maintained will reduce resazurin to pink (resorufin), whereas zones where bacteria were inhibited remain purple (non-reduced/resazurin) - record purple inhibition zones on the TLC plate as active [24]. Standard antibiotics ciprofloxacin and MeOH 12.5% were used as positive and negative controls, respectively.

2.6. Determination of Minimum Inhibitory Concentration (MIC)

Compound MICs were established via the microtiter broth dilution method as recommended by Setiawan et al. [25]. Two-fold serial dilutions were performed in 96-well plates to generate a concentration gradient of 3.9 to 500 mg/mL. To

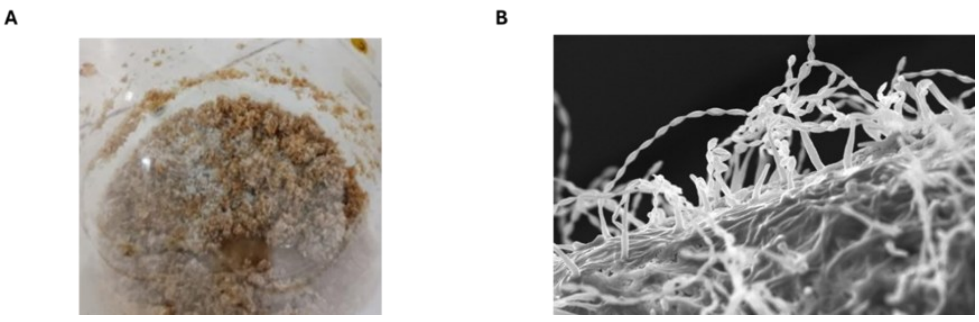

Figure 2. Solid state fermentation (a) after 14 days incubations and (b) SEM analysis of *K. palustris* 19C38A1 in shrimp shell substrate 3000 ×M.

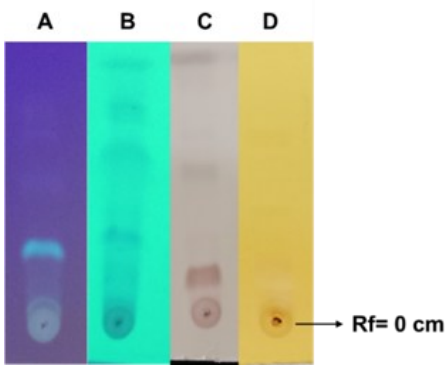

Figure 3. TLC analysis of 14 days extract of 19C38A1; (a) UV 366 nm, (b) UV 254 nm, (c) $Ce(SO_4)_2$ and (d) Dragendorff's reagent

ensure bacterial viability was unaffected by the solvent, the 12.5% MeOH was used. Overnight bacterial cultures were introduced to the wells to achieve a 200-µL final working volume. The MIC was defined as the lowest concentration yielding an optically clear well indicating complete inhibition of visible microbial growth following a 24-h incubation at 37 °C. All experiments were conducted in duplicate.

2.6. Cytotoxic Activity

The cytotoxic assay was performed to assess the cytotoxic effects of active fractions on three human cancer cell lines: lung adenocarcinoma (A549), cervical carcinoma (HeLa), and breast cancer (MCF -7) using the MTT assay [26]. The cells were grown in enriched Dulbecco's Modified Eagle Medium (DMEM) and kept at 37 °C in a humidified environment with 5% CO_2. For the assay, 7.5 x 10^3 cells were added to each well of a 96-well plate and incubated for 24 hours to facilitate cell adhesion. Subsequently, 1 µL of the stock sample solution 10 mg/mL in 100% DMSO was introduced to each well, while cells treated with 0.1% DMSO served as the solvent control. Doxorubicin 1 µL (1 mg/mL) was used as positive control. The cells were subsequently incubated for another 72 h. Following treatment, the media was substituted with 100 µL of serum-free DMEM medium that included 0.5% MTT and incubated for an additional 4 h to facilitate formazan development. The absorbance was assessed with a microplate reader at a wavelength of 570 nm. All tests were conducted in triplicate (Equation 1).

$$\%\ \text{Cell Viability} = \frac{\text{Abs Treated cells}}{\text{Abs Untreated cells}} \times 100\% \quad (1)$$

2.7. Metabolites Profiling of Active Fraction

Active fractions were dissolved in methanol, filtered using a 0.22 µm membrane, and analyzed using LC–MS/MS which was equipped with the ACQUITY UPLC® H-Class System (Waters, Beverly, MA, USA), ACQUITY UPLC® HSS C18 column (1.8 µm 2.1 × 100 mm) (Waters, Beverly, MA, USA), and Xevo G2-S Qtof Mass Spectro (Waters, Beverly, MA, USA) was linked in positive electrospray ionization mode (ESI+) [24][27]. Chromatographic separation was conducted using a gradient system of MeOH-H_2O with 0.1% formic acid, at a flow rate of 0.3 mL/min. Mass spectra were collected across an m/z range of 100–1500, utilizing data-dependent acquisition to obtain fragmentation spectra of the most intense ions. Raw data were converted using MsConvert (https://proteowizard.sourceforge.io) and dereplication was analyzed using MZmine 4.8 software (https://mzio.io) for peak identification, chromatogram construction, deconvolution, isotopic peak clustering, and sample alignment. Molecular characteristics were confirmed through comparison with online databases (KEGG, MassBank, and PubChem), and potential compound identities were allocated based on precise mass, error (ppm), and MS/MS fragmentation alignment.

2.8. Drug Likeness Properties and Biological Target Prediction

Drug-likeness and pharmacokinetic properties were analyzed using the SwissADME (http://www.swissadme.ch/) web server. In addition, toxicity and ADMET parameters were analyzed using ADMETlab 3.0 (https://admetlab3.scbdd.com/). Compound selection was

based on compliance with Lipinski's Rule of Five, gastrointestinal (GI) absorption, and predicted cytochrome P450 (CYP) enzyme inhibition profiles to assess oral bioavailability and metabolic liability. The simplified molecular-input line-entry system (SMILES) of each compound was used as input for the SwissADME analysis [28]. Furthermore, Swiss Target Prediction (http://www.swisstargetprediction.ch/) was used for initial biological target prediction [29]. Targets were prioritized according to predicted probability scores, biological relevance to antibacterial and anticancer pathways, and consistency with the dual-bioactivity hypothesis of this study.

2.9. Molecular Docking Analysis

The ligand structures were initially constructed using MarvinSketch (ChemAxon Ltd., Budapest, Hungary) and subsequently converted into three-dimensional geometries. Low-energy conformations were generated using the built-in conformer generation module, followed by geometry optimization with the MMFF94 force field to obtain energetically minimized structures suitable for molecular docking studies. Target protein structures Filamenting temperature-sensitive mutant Z (FtsZ) (PDB ID: 3VOA) and The epidermal growth factor receptor (EGFR) (PDB ID: 2J6M) were retrieved from the Protein Data Bank (PDB) (https://www.rcsb.org) and prepared in UCSF Chimera to obtain pdb file [30], where water molecules and heteroatoms were removed, hydrogen atoms were added, and Gasteiger charges were assigned. The molecular docking was performed using AutoDock Tools-1.5.7 (ADT) (https://autodocksuite.scripps.edu). Ligands were prepared by adding torsional degrees of freedom and assigning Gasteiger charges, and the receptor grids were defined around the active site residues. Docking simulations were carried out with the Lamarckian Genetic Algorithm to predict the most favorable binding conformations and binding energies with an initial population size of 50 individuals and a maximum number of energy

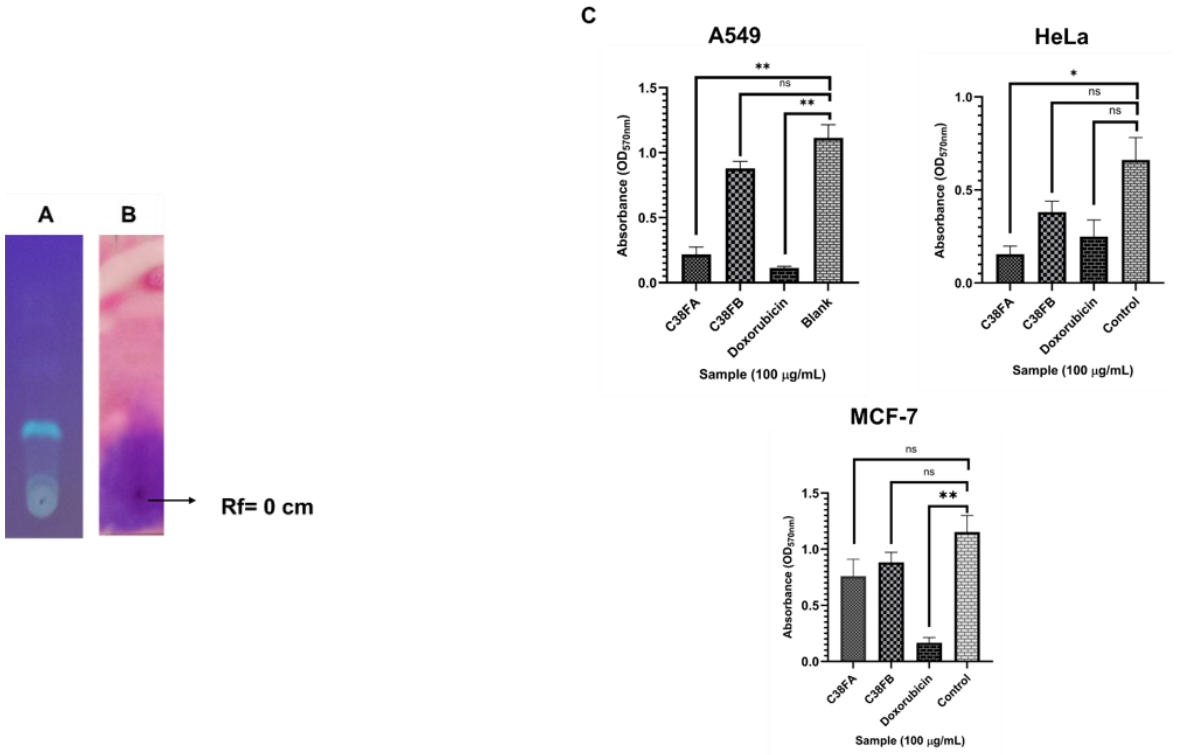

Figure 4. Bioactivity assay (a-b) TLC bioautography against MDR *S. aureus* and (c) cytotoxic activity of C38FA and C38FB (100 µg/mL) against A549, HeLa, and MCF-7 cancer cell lines determined by MTT assay (OD_{570nm}). Data are presented as mean ± SD (n = 3). Statistical analysis was performed using one-way ANOVA followed by Dunnett's multiple comparisons test comparing each treatment with the corresponding blank control. $p < 0.05$, $p < 0.01$; ns, not significant.

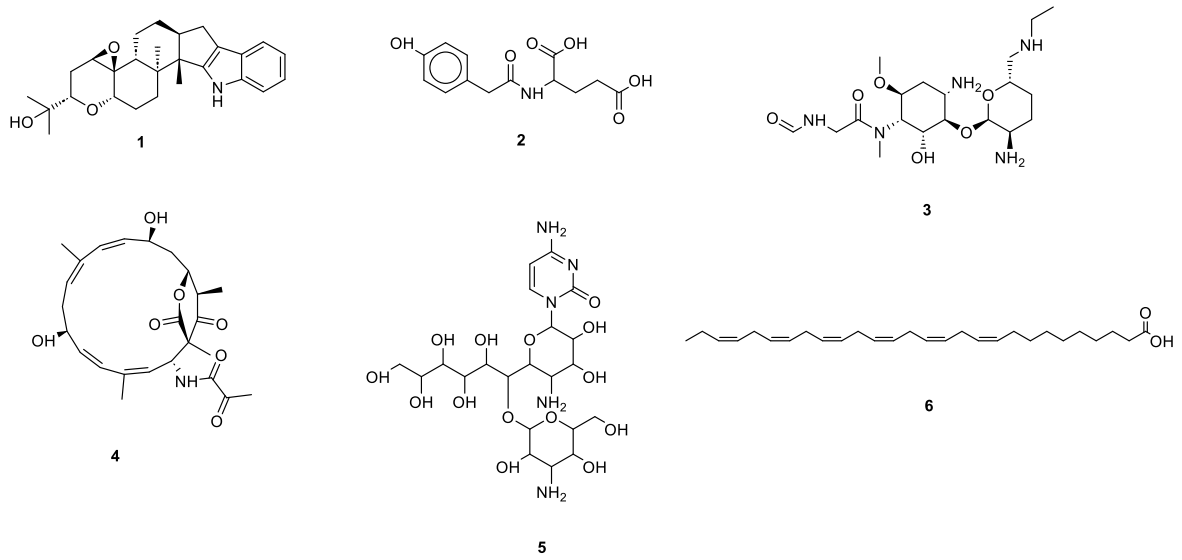

Figure 5. Bioactive compounds of C38FA.

evaluations set to 2,500,000. The ligand was treated as flexible, while the receptors were regarded as rigid. The grid box dimensions for the FtsZ receptor were 40 × 40 × 40 Å with a spacing of 0.375Å and centered at coordinates x =3.677, y = -6.693, z = 21.066, encompassing the active-site residues. For EGFR the grid box dimensions were 40 × 56 × 40 Å, with a spacing of 0.375 Å and centered at x = 20.340, y = 2.395, z = -22.537, covering the co-crystallized ligand binding pocket.

Prior to screening the test compounds, the docking protocol was validated by extracting and redocking the co-crystallized native ligands back into their respective binding sites using identical parameters. The protocol's accuracy was confirmed by a root mean square deviation (RMSD) of ≤ 2.0 Å between the docked pose and the experimental crystal structure. Following validation, the test compounds and reported positive controls were docked to evaluate binding affinities and conformational consistency. The resulting complexes were analyzed utilizing BIOVIA Discovery Studio Visualizer to characterize key binding modes, including hydrogen bonding and hydrophobic interactions [31]–[33].

2.10. Statistical Analysis

Data are presented as mean ± standard deviation (SD). Statistical analyses were conducted using GraphPad Prism v10 (GraphPad Software, USA).

3. RESULTS AND DISCUSSIONS

3.1. Isolates of Actinomycetes

The morphological characteristics of the isolate 19C38A1 are consistent with those of filamentous actinomycetes. Macroscopically, the colony exhibits a dry, chalky, and opaque surface indicative of active sporulation (Figure 1(a)). Microscopically, the isolate forms an extensive network of long, thin, septate hyphae that branch profusely to produce both substrate and aerial mycelia. Several hyphal tips show developing spore chains, a hallmark reproductive feature of actinomycetes (Figure 1(b)). Together, the colony texture, pigmentation, filamentous growth, and spore-chain formation confirm that this isolate possesses the defining developmental traits of actinomycetes capable of synthesizing diverse bioactive secondary metabolites. In our previous study, the sequencing of the 16S rDNA gene indicated the genus Kocuria. The new isolate, *Kocuria palustris* 19C38A1, was identified via sequencing with a similarity percentage of 99.77% and was successfully registered in GenBank with access number LC659429 [21].

3.2. Solid State Fermentation

After 14 days of SSF, *K. palustris* 19C38A1 grew vigorously on a shrimp-shell substrate. The macroscopic appearance (Figure 2(a)) consists of thick mycelial growth forming a compact pale-

cream matrix on the chitin-rich surface. Localized softening and visible degradation zones point to an active enzymatic attack on both chitin and protein components, which agrees with literature that states morphological and metabolic differentiation is induced in actinomycetes by chitin-based substrates [34].

SEM imaging (Figure 2(b)) revealed an extensive network of filamentous hyphae emerging from the substrate. The hyphae exhibited uniform diameter, frequent branching, and prominent spore-bearing structures characteristic of mature actinomycete development. The presence of elongated, twisted spore chains suggests that *K. palustris* undergoes complete reproductive differentiation under SSF conditions, reflecting strong environmental induction by the shrimp-shell matrix. Deep hyphal penetration into the substrate further highlights efficient enzymatic modification of chitin-mineral complexes, which are known to act both as nutrient sources and as triggers of secondary metabolite biosynthesis [35]. The robust filamentation and sporulation, as observed here, agree with the previously reported increased production of alkaloidal, polyketide, and peptide metabolites under chitin-enriched fermentation systems. Overall, both macroscopic and ultrastructural morphology exhibits that shrimp shell waste provides an optimal ecological mimic for the development of *K. palustris* 19C38A1.

3.3. TLC Identification of Crude Extract

The result of 14 days fermentation of 19C38A1 isolates on shrimp shell media could induce the production of secondary metabolites which have characteristic in UV 366 (Figure 3(a)), UV 254 nm (Figure 3(b)), and various of bioactive compound with different Rf value (Figure 3(c)) especially alkaloid derivative compoud which have characetristic as yellow colour at Rf = 0 (Figure 3 (d)). It is related to the report of Ma et al. [20] chitin -based media could express gene of alkaloid compound from microorganisms.

3.4. Antibacterial and Cytotoxicity

Meanwhile, the antibacterial activity at shown Rf = 0 which is the very polar compound possesed the inhibition of MDR *S. aureus* after sprayed with resazurin 0.05% (Figures 4(a) – 4(b)). The blue–purple region after resazurin treatment indicates suppressed metabolic activity of MDR *S. aureus*, confirming that the polar fraction contains potent antibacterial components [36]. The minimum inhibitory concentration (MIC) assay revealed that C38FA exhibited antibacterial activity with an MIC of 250 µg/mL, whereas C38FB was inactive. In cytotoxicity assays (Figure 4(c)), C38FA significantly reduced cell viability in A549 and HeLa cells compared with the respective blank controls ($p < 0.01$ and $p < 0.05$, respectively; one-way ANOVA followed by Dunnett's test), corresponding to growth inhibition rates of 89 ± 0.057% and 98 ± 0.043%. In contrast, although C38FA exhibited a 40 ± 0.453% reduction in MCF-7 cell viability, this effect was not statistically significant ($p > 0.05$). Meanwhile, the non-polar fraction C38FB did not produce a statistically significant cytotoxic effect in any of the tested cancer cell lines ($p > 0.05$), indicating limited anticancer activity under the experimental conditions.

At the tested concentration, C38FA achieved up to 98% inhibition, comparable to the 100% inhibition observed for doxorubicin under identical conditions, indicating substantial cytotoxic potency, particularly against HeLa and A549 cells. Although

Table 1. Bioactive compound from active fraction C38FA

No	Compound Name	Formula	*m/z*	Adduct	D ppm
1	Terpendole B	$C_{27}H_{35}NO_3$	422.2552	$[M+H]^+$	-0.014
2	*p*-Hydroxyphenylacetylglutamic acid	$C_{13}H_{15}NO_6$	281.0899	$[M+Na]^+$	+0.222
3	Istamycin C1	$C_{19}H_{37}N_5O_6$	432.2810	$[M+H]^+$	-0.001
4	Lankacidin C	$C_{18}H_{34}N_4O_{11}$	448.2455	$[M+Na]^+$	+0.045
5	Anthelmycin	$C_{21}H_{37}N_5O_{14}$	584.4737	$[M+H]^+$	+0.232
6	(10Z,13Z,16Z,19Z,22Z,25Z)-Octacosa-10,13,16,19,22,25-hexaenoic acid	$C_{28}H_{44}O_2$	413.2686	$[M+H]^+$	-0.073

Table 2. ADME prediction of active fraction C38FA.

Compound	GI	BBB	Pgp	CYP1A2	CYP2C19	CYP2C9	CYP2D6	CYP3A4	Lipinski
	absorption	permeant	substrate	inhibitor	inhibitor	inhibitor	inhibitor	inhibitor	
1	High	Yes	No	Yes	No	No	No	No	Yes
2	High	No	No	No	No	No	No	No	Yes
3	Low	No	Yes	No	No	No	No	No	Yes
4	Low	No	Yes	No	No	No	No	No	Yes
5	Low	No	Yes	No	No	No	No	No	No
6	Low	No	Yes	No	No	No	No	No	No

slightly less potent than the positive control, the observed activity supports its potential as a promising bioactive candidate. Previous reports indicate that many marine-derived natural products exhibit biologically relevant antimicrobial and cytotoxic activities within the low concentration range during preliminary screenings [37], placing the activity of C38FA within an acceptable range for early-stage evaluation.

The presence of metabolites with dual biological functionality, a characteristic of many actinomycete -derived natural products, is highlighted by the convergence of robust antibacterial activity and prominent cytotoxicity in C38FA as active fraction. Due to common metabolic weaknesses, compounds that can interfere with vital bacterial functions like protein synthesis, membrane integrity, or redox balance frequently show parallel effects against cancer cells [38]. Future studies should therefore focus on compound isolation and structural elucidation, bioactivity-guided fractionation, and validation using mechanistic and *in vivo* models. Based on these results, C38FA was selected for subsequent metabolite identification.

3.5. Profilling of Active Fraction

Profiling of the bioactive fractions obtained from actinomycetes cultivated on shrimp-shell waste medium revealed the presence of six structurally diverse secondary metabolites with known antibacterial or cytotoxic relevance (Figure 5). Based on high-resolution mass spectrometry, the dominant ion features were putatively annotated as terpendole B ($C_{27}H_{35}NO_3$; *m/z* 422.2552; Δppm –0.014), *p*-hydroxyphenylacetylglutamic acid ($C_{13}H_{15}NO_6$; *m/z* 281.0899; Δppm +0.222), istamycin C_1 ($C_{19}H_{37}N_5O_6$; *m/z* 432.2810; Δppm –0.001), lankacidin C ($C_{25}H_{33}NO_7$; *m/z* 448.2455; Δppm +0.045), anthelmycin ($C_{21}H_{37}NO_{14}$; *m/z* 584.4737; Δppm +0.232), and the long-chain fatty acid octacosa-10,13,16,19,22,25-hexaenoic acid ($C_{28}H_{44}O_2$; *m/z* 413.2686; Δppm –0.073). The extremely low mass errors ($|\Delta ppm| < 0.3$) across the dataset support high confidence in mass assignments and structural annotation (Table 1).

Notably, several of the detected metabolites terpendole B, istamycin C1, lankacidin C, and anthelmycin are well-established natural products with potent antibacterial or cytotoxic properties, consistent with the biological activity observed in the active fractions [39]–[42]. While further targeted isolation is required to definitively identify the active principles responsible for the observed efficacy, The presence of both peptide-based antibiotics (e.g., istamycins and lankacidins) and alkaloidal or polyketide-derived compounds highlights the broad biosynthetic capacity of actinomycetes when cultivated on a nutrient-rich chitinous waste substrate.

Comparing the bioactivities of the identified metabolites with those previously reported, compound **1** has been found to be cytotoxic to various human cancer cell lines, which matches the cytotoxic activity. Compound **3**, a known aminoglycoside antibiotic and compound **4** a polyketide antibiotic are likely responsible for antibacterial activity, especially against Gram-positive bacteria [43]–[45]. On the other hand, compounds **2** and **5** have limited documented biological activities, but their presence together may work together to produce the combined antibacterial and cytotoxic effects noted.

Table 3. Predicted ADMET and toxicity profiles of compounds **1–6** calculated using ADMETlab 3.0. Probability values range from 0 to 1, where higher values indicate a greater likelihood of the predicted pharmacokinetic or toxicity endpoint.

Category	Parameter	1	2	3	4	5	6	Interpretation
Absorption	Caco-2 permeability	−4.89	−6.01	−5.44	−5.10	−5.89	−4.99	Values > −5.15 indicate acceptable intestinal permeability; compounds 1 and 6 show favorable absorption potential.
	HIA	0.0	0.0	0.3	0.0	1.0	0.0	Lower probability values indicate high intestinal absorption; most compounds are predicted to be well absorbed except compound 5.
	Oral bioavailability (F50%)	0.807	0.508	0.962	0.991	0.998	0.383	Higher values suggest improved oral exposure; compounds 3–5 exhibit favorable oral bioavailability.
Distribution	PPB (%)	92.05	54.00	29.94	43.83	16.24	98.32	High PPB (>90%) may reduce free drug fraction; compounds 1 and 6 show extensive plasma protein binding.
	BBB penetration	0.984	0.001	0.002	0.007	0.001	0.037	Values close to 1 indicate BBB permeability; only compound 1 is predicted to cross the BBB efficiently.
Metabolism	CYP3A4 substrate	1.0	0.0	0.9	0.0	1.0	0.0	Value ≈1 indicates metabolism via CYP3A4, suggesting possible hepatic metabolism and drug–drug interaction risk.
Excretion	Clearance (mL/min/kg)	10.75	4.13	2.13	11.53	0.88	4.19	Moderate clearance (5–15) suggests balanced elimination; low values indicate prolonged systemic exposure.
	Half-life (h)	0.92	1.75	1.53	1.49	2.36	0.31	Short predicted half-life (<3 h) indicates rapid systemic elimination.
Cardiotoxicity	hERG blocker	0.339	0.005	0.194	0.015	0.008	0.780	Higher probability indicates cardiotoxicity risk; compound **6** shows elevated predicted hERG liability.
Hepatotoxicity	DILI	0.45	0.58	0.05	0.55	0.24	0.0	Moderate probabilities suggest potential liver toxicity requiring experimental validation.

Table 3. *Cont.*

Category	Parameter	1	2	3	4	5	6	Interpretation
Genotoxicity	AMES	0.766	0.025	0.215	0.203	0.787	0.938	Higher values indicate potential mutagenicity risk; compounds 1, 5, and 6 show elevated probabilities.
Systemic toxicity	Acute oral toxicity	0.934	0.159	0.192	0.030	0.076	0.007	Higher probability indicates increased systemic toxicity risk; compound 1 shows highest predicted toxicity.
Organ toxicity	Nephrotoxicity	0.506	0.290	0.837	0.828	0.227	0.044	Elevated probabilities suggest possible kidney toxicity concerns.
	Neurotoxicity	0.487	0.174	0.904	0.072	0.866	0.001	Higher values indicate potential CNS toxicity risk.
Other toxicity	Skin sensitization	0.989	0.583	0.995	1.0	0.005	1.0	Values near 1 indicate likely skin sensitizers.
	Carcinogenicity	0.382	0.095	0.130	0.155	0.043	0.0	Low-to-moderate probabilities suggest limited carcinogenic risk overall.

3.6. Drug Likeness and Biological Target Prediction

Analysis of the top six candidates revealed distinct differences in their predicted pharmacokinetic properties (Table 2). Compounds **1** and **2** displayed high gastrointestinal absorption, whereas Compounds **3–6** were characterized by low absorption, indicating that the latter group may require structural refinement to improve oral bioavailability. Among the set, only Compound **1** was predicted to cross the blood–brain barrier, consistent with generally limited central nervous system penetration for the remaining molecules. Efflux susceptibility varied, compounds **4–6** identified as P-glycoprotein substrates, in contrast to compounds **1–3**, which are not expected to undergo significant P-gp–mediated transport. With respect to metabolic liability, none of the compounds were predicted to inhibit CYP2C19, CYP2C9, CYP2D6, or CYP3A4, suggesting a broadly low propensity for cytochrome P450–related drug–drug interactions. Only compound **1** showed predicted inhibitory activity toward CYP1A2, whereas Compounds **2–6** were classified as non-inhibitors.

According to ADME, compounds **1** and **2** present the clearest paths toward dual antibacterial/cytotoxic development (with compound-specific caveats), Compound **3** is a viable secondary candidate pending exposure strategy, and compounds **4–6** are currently limited by efflux and permeability constraints. Compounds **1** and **2** demonstrates that *K. palustris* 19C38A1 grown on shrimp shell media can be promising leads for further preclinical evaluation. The rule predicts favorable oral bioavailability for molecules with molecular weight ≤500 Da, logP ≤5, hydrogen bond donors ≤5, and hydrogen bond acceptors ≤10 [46]. Compounds **1** and **2** generally conform to these criteria, consistent with their predicted high gastrointestinal absorption. In contrast, Compounds **3–6** likely violate one or more parameters due to increased polarity, molecular size, or lipophilicity, contributing to reduced absorption and P-glycoprotein susceptibility [47]. Such deviations are common among natural products and macrocyclic scaffolds, which often occupy chemical space beyond the Rule of Five while retaining biological activity through alternative transport or conformational mechanisms [48]. These findings not only underscore the value of shrimp-shell waste as an enabling fermentation platform for natural

product discovery but also highlight the broader prospect of converting marine by-products into a renewable source of drug-like bioactive scaffolds.

The observed pharmacokinetic trends are strongly supported by structure–ADMET relationships identified through *in silico* analysis (Table 3). Compounds with greater lipophilic character of compounds **1** and **6** exhibited improved Caco-2 permeability and predicted intestinal absorption, consistent with enhanced passive diffusion across biological membranes. In contrast, the highly polar architectures of compounds **2** and **3**, characterized by abundant hydrogen-bond donors and acceptors, were associated with reduced membrane permeability, reflecting limited transcellular transport typical of polar natural products. Despite this limitation, favorable human intestinal absorption probabilities suggest that carrier-mediated or paracellular transport mechanisms may contribute to systemic uptake. Macrocyclic frameworks represented compounds **4** and **5** displayed comparatively high predicted oral bioavailability, likely arising from conformational flexibility and intramolecular hydrogen bonding that effectively mask polarity despite large molecular size. Distribution analysis further indicated extensive plasma protein binding for lipophilic compounds **1** and **6**, whereas only compound **1** demonstrated substantial blood–brain barrier permeability, consistent with physicochemical parameters governing central nervous system exposure, including balanced polarity and hydrophobicity [49].

Furthermore, metabolic and toxicity predictions further underscored clear structure–ADMET relationships relevant to pharmacological development. Compounds **1**, **3** and **5** were predicted CYP3A4 substrates, indicating susceptibility to hepatic oxidative metabolism and potential drug–drug interactions, while the polar compound **2** is more likely to undergo phase II conjugative metabolism and compound **6** may be processed through fatty-acid metabolic pathways. Predicted clearance and half-life values suggested relatively rapid systemic elimination, particularly for polar molecules prone to renal excretion [50]. Toxicity profiling identified an elevated probability of hERG channel inhibition for compound **6**, plausibly linked to its extended hydrophobic chain facilitating interactions with membrane-embedded ion channels [51]. Moderate hepatotoxicity and mutagenicity alerts observed across several compounds may reflect the formation of reactive metabolic intermediates derived from conjugated or lipophilic structural motifs [52]. Additionally, increased nephrotoxicity predictions for compounds **3** and **4** are consistent with the renal accumulation commonly observed for polar antibiotic scaffolds.

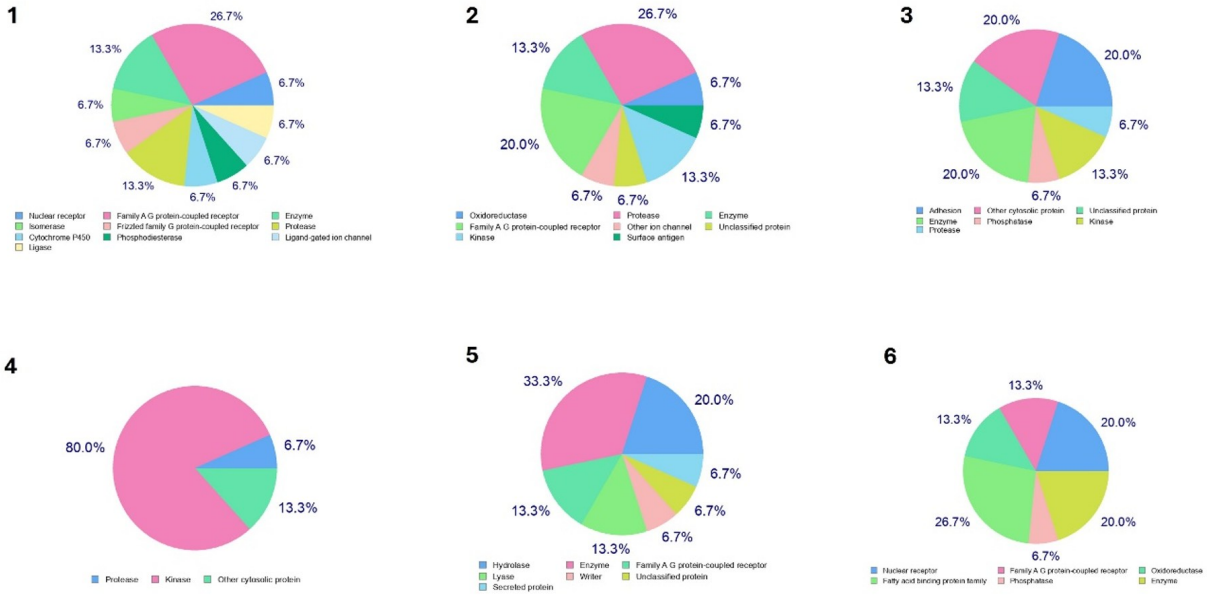

Figure 6. Pie chart of biological target of the compounds **1**–**6**.

Table 4. Docking analysis against FtsZ and the compounds interactions.

No	Energy affinity (Kcal/mol)	Interactions
1	-6.89	Thr133*, Glu139*, Phe183#, Ala26#
2	-5.75	Gly108*, Ala73*, Met105*. Thr133*, Gly110*, Arg143, Glu139
3	-5.78	Ser103*, Val19*, Gly23*, Gly104*, Gly107*, Arg143*, Glu139, Met179#, Phe183#
4	-5.97	Asn25*, Gly107*, Gly104*, Gly23*, Gly22*, Met179#, Met180#, Phe183#, Gly139
5	-3.96	Asn25*, Asn166*, Met105*, Gly107*, Val19* Gly110*, Gly 22*, Gly21
6	-3.76	Phe136#, Phe183#, Pro135#, Ala71#
Ciproloxacin	-8.23	Gly22*, Gly23*, Gly110*, Thr109*, Gly72*, Ala71*, Val19, Arg143

* Hydrogen bonding, # Hydrophobic bonding

Collectively, these findings highlight the intrinsic pharmacokinetic trade-off in natural product scaffolds, whereby lipophilicity enhances permeability and tissue distribution at the cost of increased toxicity liability, whereas polarity improves safety profiles but limits absorption efficiency, emphasizing the need for rational structural optimization to achieve balanced drug-like properties [53][54].

Analysis of the six top bioactive compounds revealed diverse but biologically relevant target classes that strongly support their dual antibacterial and anticancer potential (Figure 6). Compounds **1**, **2**, **3**, **5**, and **6** showed mixed affinity toward GPCRs, enzymes, kinases, oxidoreductases, and phosphatases, reflecting broad biochemical interactions that may contribute to their antibacterial activity against MRSA [55].

In particular, the presence of kinases, proteases, oxidoreductases, and phosphodiesterases among predicted targets aligns with essential MRSA survival pathways, including cell wall remodeling, redox homeostasis, and signal transduction. These classes are frequently exploited by antibacterial agents, indicating that the compounds can disrupt multiple bacterial processes simultaneously [55]. Notably, compound **4** exhibited a highly focused profile, with 80% of predicted targets belonging to the protease class, suggesting strong potential to inhibit bacterial proteases critical for MRSA virulence and resistance.

Furthermore, all six compounds displayed predicted affinity toward kinase-related or EGFR-associated protein families, supporting their observed cytotoxicity. The presence of nuclear receptors, fatty-acid-binding proteins, and phosphatases among predicted targets for compounds **5** and **6** further reinforces their ability to modulate human signaling pathways relevant to cancer progression. Overall, the SwissTarget profiles indicate that these compounds possess dual bioactivity target interactions, enabling them to act as dual-target agents by simultaneously inhibiting MRSA-related enzymes and interacting with EGFR -associated kinase pathways responsible for cytotoxic effects.

3.7. Molecular Docking Analysis

The active fraction C38FA was computationally evaluated against antibacterial and anticancer molecular targets using molecular docking analysis (Figures 7 – 8). The result for antibacteria assay, the compounds exhibited predicted binding affinities toward the FtsZ receptor (Table 4). FtsZ in *Staphylococcus aureus* (FtsZ) is a crucial, tubulin -like protein that polymerizes with GTP to form the Z-ring, directing bacterial cell division (cytokinesis) [56]. It's a major target for new antibiotics because inhibiting it disrupts cell division, causing enlarged cells.

Molecular docking of the six test compounds against FtsZ revealed binding energies ranging from –3.76 to –6.89 kcal/mol (Figure 7), with compound **1** showing the strongest affinity at –6.89 kcal/mol, approaching the reference antibiotic ciprofloxacin (–8.23 kcal/mol). Compound **1** formed key interactions with Thr133, Glu139, Phe183, and Ala26, suggesting a potentially stable binding mode within the FtsZ active site. Compounds **2**, **3**, and **4** displayed moderate affinities (–5.75, –5.78, –5.97 kcal/mol) and engaged several important residues such as Gly108, Met105, Thr133, Gly110, Ser103,

Val19, Gly23, Gly104, Gly107, Arg143, and Phe183, indicating reasonable compatibility with the polymerization interface. In contrast, compounds **5** and **6**, with weaker scores (–3.96 and –3.76 kcal/mol), interacted with fewer critical residues and lacked strong hydrophobic or hydrogen-bonding contacts, reducing their inhibitory potential. Ciprofloxacin demonstrated the greatest stabilizing interactions, forming an extensive network with Gly22, Gly23, Gly110, Thr109, Gly72, Ala71, Val19, and Arg143, explaining its superior affinity. Overall, compound **1** is predicted to possess the most favorable binding profile among the tested compounds among the tested molecules for inhibiting FtsZ, while compounds **2**–**4** show moderate potential and compounds **5**–**6** are less likely to exert significant inhibitory activity. The robust FtsZ binding affinity of compounds **1**, **3**, and **4** stems from their ability to mimic the established interaction profile of ciprofloxacin. Specifically, these compounds anchor at the polymerization interface (Val19–Gly23), stabilize the critical glycine-rich loop (Gly104, Gly107, Gly110), and engage in hydrophobic packing with Met179 and Phe183 [57] [58].

This targeted localization provides a direct structural rationale for the compounds' antibacterial efficacy. FtsZ drives bacterial cytokinesis through GTP-dependent polymerization into a contractile Z-ring [59]. Our models suggest that by binding these specific interface regions, the compounds restrict the conformational dynamics essential for protofilament elongation and compromise the lateral association of FtsZ monomers. The resulting failure in Z-ring assembly precludes proper septum formation. Consequently, this structural interference induces cellular filamentation and arrests cell division, mechanistically coupling the in silico binding interactions to the observed antimicrobial phenotype [60].

While FtsZ docking elucidates the antibacterial mechanism, the active fraction's concurrent cytotoxicity in cancer cells necessitated investigating an oncogenic target. We therefore selected EGFR, given its pivotal role in driving tumor proliferation, survival, and resistance [61]. Molecular docking of the six compounds against EGFR produced binding energies ranging from –3.75 to –9.03 kcal/mol (Figure 8), with compound **1** displaying the strongest affinity (–9.03 kcal/mol), approaching the potency of the reference ligand doxorubicin (–9.28 kcal/mol). Compound **1** formed extensive interactions with several key residues within the EGFR active site, including Asp855, Lys745, Thr854, Phe723, Val726, Ala743, Leu718, Met793, and Leu844, indicating strong stabilization within the kinase domain. Compound **4** also showed high affinity (–7.37 kcal/mol) and interacted with crucial residues such as Met793, Cys797, Cys775, Leu844, Val726, and Ala743, suggesting effective occupation of the ATP-binding pocket. Moderate binding was observed for compounds **3** and **5** (–5.92 and –4.15 kcal/mol), which engaged residues including Asn842, Cys797, Asp855, Glu762, Lys745, and Met793, indicating partial compatibility with the EGFR active site but less extensive stabilization compared with compounds **1** and **4**. The weakest affinities were shown by compounds 2 and 6 (–3.94 and –3.75 kcal/mol),

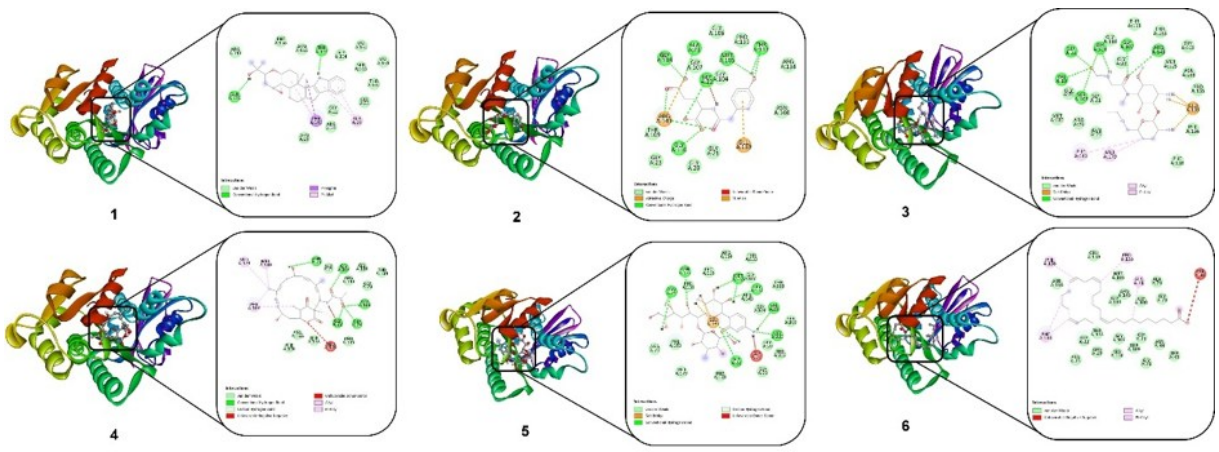

Figure 7. Binding pose of active fraction compounds with residue of the FtsZ receptor.

Table 5. Docking analysis against EGFR and the compounds interactions.

Compounds	Energy affinity (kcal/mol)	Interactions
1	-9.03	Asp855*, Lys745*, Thr854*, Phe723#, Val726#, Ala743#, Leu718#, Met793#, Leu844#
2	-3.94	Lys745, Glu762, Met793, Val726
3	-5.92	Asn842*, Cys797*, Asp855, Glu762, Lys745
4	-7.37	Met793*, Cys797*, Cys775#, Leu844#, Val726#, Ala743#, Leu718#,
5	-4.15	Lys745*, Glu762*, Cys797*, Asp800*, Met793*, Val726#
6	-3.75	Met783#, Leu844#, Leu718#, Val726#, Ala743#, Lys745
Doxorubicin	-9.28	Met793*. Gln791*, Arg841*, Ala743#, Leu718#, Leu844#, Val726#, Lys745#

* Hydrogen bonding, # Hydrophobic bonding

whose limited interactions primarily with Lys745, Glu762, Met793, Val726, Leu844, Leu718, and Ala743 suggest insufficient engagement of key catalytic residues to serve as strong inhibitors. The reference ligand doxorubicin demonstrated broad interaction coverage, including Met793, Gln791, Arg841, Ala743, Leu718, Leu844, Val726, and Lys745, supporting its superior affinity (Table 5).

The strong EGFR binding affinity of the compounds, particularly compounds **1** and **4**, results from their ability to mimic key interactions observed with doxorubicin. Both compounds effectively anchor to the hinge region through contacts with Met793, Ala743, and Leu718, while also stabilizing the catalytic site via Lys745 [62]. Their engagement with hydrophobic core residues such as Val726 and Leu844 further enhances binding stability [62]. Additionally, compound **1** interacts with activation-loop residues Asp855 and Thr854, supporting inhibitory potential. Compound **4** provides an extra advantage by approaching the covalent pocket near Cys797, contributing to its strong overall affinity.

The preferential localization of compounds **1** and **4** within the EGFR kinase domain provides a robust structural rationale for the active fraction's observed cytotoxicity. Our models suggest that these compounds act as competitive inhibitors by directly occupying the ATP-binding pocket and sterically restricting activation loop dynamics. This structural blockade is predicted to abrogate EGFR autophosphorylation, thereby uncoupling the receptor from critical downstream oncogenic cascades, including the PI3K/AKT and MAPK/ERK pathways [63]. The consequent withdrawal of these essential survival signals provides a mechanistic basis for the induction of cell cycle arrest and apoptosis, directly linking the potent in silico binding profiles to the *in vitro* anti-cancer phenotype.

Structural comparison revealed that several tested compounds share common pharmacophoric features with known FtsZ and EGFR inhibitors, including aromatic ring systems, hydrogen bond donor/acceptor functionalities, and hydrophobic moieties that facilitate interaction within conserved binding pockets [64]. These features resemble interaction motifs reported for ciprofloxacin in FtsZ and doxorubicin within the EGFR kinase domain, particularly involving hinge-region anchoring and hydrophobic pocket occupation [65][66]. Such similarities support the predicted binding modes and provide a mechanistic rationale for the observed docking affinities, although experimental validation remains necessary to confirm inhibitory activity. These docking results provide theoretical insights into possible ligand–protein interactions and should be interpreted as predictive rather than definitive evidence of biological inhibition.

4. CONCLUSIONS

Marine-derived actinobacteria represent a rich source of chemically diverse secondary metabolites with therapeutic potential. In this study, shrimp shell–based solid-state fermentation (SSF) supported the growth of *K. palustris* 19C38A1 and promoted the production of bioactive metabolites. To our knowledge, this is the first report demonstrating that shrimp-shell waste can serve as a fermentation substrate to stimulate secondary metabolism in *K. palustris*. Partially purified

fractions exhibited antibacterial activity against multidrug-resistant *S. aureus* (MIC 250 µg/mL) and cytotoxic effects toward A549 (89 ± 0.057%) and HeLa (98 ± 0.043%) cells. These findings suggest that shrimp shell–driven SSF enhances the biosynthesis of metabolites with dual antibacterial and anticancer potential, although activity cannot yet be attributed to individual compounds. Untargeted metabolomics tentatively identified six putative metabolites: terpendole B (**1**), *p*-hydroxyphenylacetylglutamic acid (**2**), istamycin C1 (**3**), lankacidin C (**4**), anthelmycin (**5**), and (10Z,13Z,16Z,19Z,22Z,25Z)-octacosahexaenoic acid (**6**). Their presence indicates activation of nitrogen-containing and polyketide-associated biosynthetic pathways under shrimp-shell fermentation conditions. Furthermore, molecular docking revealed binding affinities toward FtsZ (−3.76 to −6.89 kcal/mol) and EGFR (−3.75 to −9.03 kcal/mol). *In silico* ADME profiling further indicated that the annotated compounds possess physicochemical properties, particularly lipophilicity and molecular weight, compatible with cellular permeability. Notably, compounds showing stronger docking affinities corresponded to greater observed biological activity. The antibacterial activity is mechanistically supported by predicted interactions at the FtsZ polymerization interface, whereas occupation of the EGFR ATP-binding pocket provides a plausible explanation for the observed cytotoxicity in cancer cell lines. However, important limitations remain. Bioactivity assays were conducted on partially purified fractions, metabolite identities are tentative, and mechanistic interpretations rely on computational predictions without experimental validation. Future studies should focus on compound isolation, structural confirmation, target-specific validation, and in vivo evaluation, alongside fermentation scale-up. Collectively, these findings highlight shrimp-shell waste as a sustainable substrate for activating microbial secondary metabolism and support marine by-product–based fermentation as a promising strategy for expanding access to drug-like natural product scaffolds.

AUTHOR INFORMATION

Corresponding Author

Widyastuti Widyastuti — Department of Chemistry, Lampung University, Bandar Lampung-35145 (Indonesia);
orcid.org/0000-0003-2328-5777
Email: widyastuti@fmipa.unila.ac.id

Authors

Fendi Setiawan — Doctoral Program, Lampung University, Bandar Lampung-35145 (Indonesia);
orcid.org/0000-0003-1006-5150

Ety Apriliana — Medical Microbiology, Lampung University, Bandar Lampung-35145 (Indonesia);
orcid.org/0000-0002-6202-461X

Wawan A. Setiawan — Department of Biology, Lampung University, Bandar Lampung-35145 (Indonesia);
orcid.org/0000-0003-1602-9951

Peni Ahmadi — Research Center for Vaccine

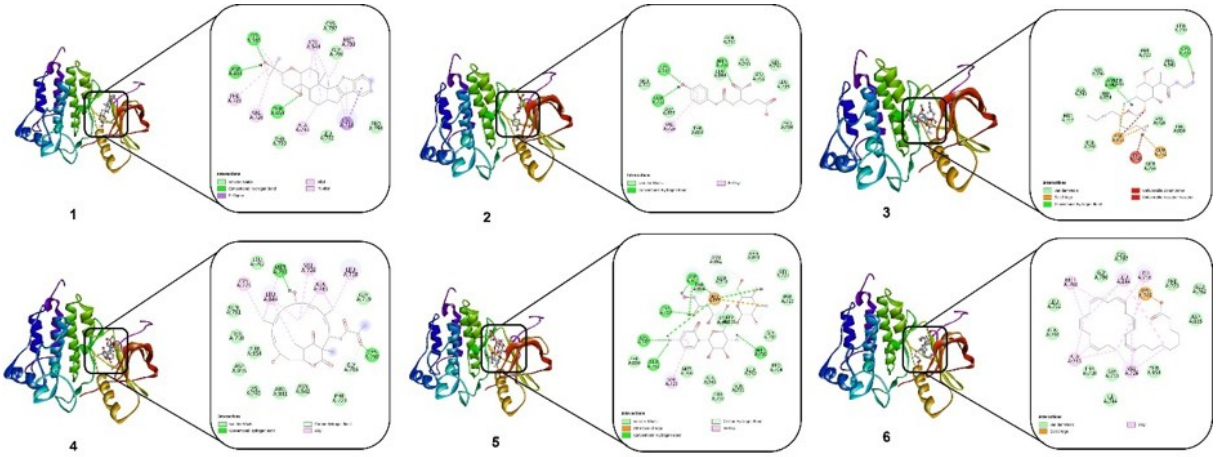

Figure 8. Binding pose of active fraction compounds with residue of the EGFR receptor.

and Drugs, National Research and Innovation Agency, Cibinong-16911 (Indonesia);
orcid.org/0000-0002-6448-3959

Author Contributions

Conceptualization, Writing Original Draft Preparation, J. H., F.S.; Software, Visualization, F. S.; Validation, N. L. G. R. J., P. A.; Methodology, Formal Analysis, Investigation, Data Curation, F. S., P. A.; Resources, Writing Review & Editing, J. H., P. A.; Supervision, Funding Acquisition, J. H. ; Project Administration, N. L. G. R. J., E. A., W. W.

Conflicts of Interest

The authors declare no conflict of interest.

ACKNOWLEDGEMENT

This research was supported by the Higher Education Technology Innovation Lampung University (HETI UNILA), Asian Development Bank, Directorate General of Higher Education, Research and Technology, the Ministry of Education, Culture, Research and Technology, Republic of Indonesia, for the Innovation Research Scheme and Domestic Cooperation award with a grant number 6044/UN26/HK.01.03/2022. The authors also thank Ester Monika Simarmata for maintaining the actinobacteria, the Technical Service Unit, Integrated Laboratory (UPA LT), Lampung University and Genomics and Cryo-EM Building National Research and Innovation Agency (BRIN) for providing the research facilities.

DECLARATION OF GENERATIVE AI AND AI-ASSISTED TECHNOLOGIES IN THE MANUSCRIPT PREPARATION

During the preparation of this work the authors used Microsoft Copilot to assist in language editing, structuring, and improving clarity of the manuscript. After using this tool, the authors reviewed and edited the content as needed and took full responsibility for the content of the publication.

REFERENCES

[1] I. Gajic, N. Tomic, B. Lukovic, M. Jovicevic, D. Kekic, M. Petrovic, M. Jankovic, A. Trudic, D. M. Culafic, M. Milenkovic, and N. Opavski. (2025). "A Comprehensive Overview of Antibacterial Agents for Combating Multidrug-Resistant Bacteria: The Current Landscape, Development, Future Opportunities, and Challenges". *Antibiotics.* **14** (3): 221. 10.3390/antibiotics14030221.

[2] K. Ruzindana and R. I. Anorlu. (2025). "Global Disparities in Gynecologic Cancer Outcomes: A Call for Action". *International Journal of Gynecology and Obstetrics.* **171** (S1): 210-220. 10.1002/ijgo.70278.

[3] A. Abdulhak, H. H. Zedan, H. A. El-Mahallawy, A. A. Sayed, H. O. Mohamed, and M. M. Zafer. (2025). "Multidrug-Resistant Pseudomonas Aeruginosa in Immunocompromised Cancer Patients: Epidemiology, Antimicrobial Resistance, and Virulence Factors". *BMC Infectious Diseases.* **25** (1): 804. 10.1186/s12879-025-11182-0.

[4] R. Zhang, S. F. Tan, Y. Wang, J. Wu, and C. Zhang. (2025). "From Macrophage Polarization to Clinical Translation: Immunomodulatory Hydrogels for Infection-Associated Bone Regeneration". *Frontiers in Cell and Developmental Biology.* **13**. 10.3389/fcell.2025.1684357.

[5] M. P. Narsing Rao, S. R. Quadri, M. Sathish, N. T. Quach, W. J. Li, and A. Thamchaipenet. (2025). "Exploring Omics Strategies for Drug Discovery from Actinomycetota Isolated from the Marine Ecosystem". *Frontiers in Pharmacology.* **16**. 10.3389/fphar.2025.1634207.

[6] L. T. Tan. (2023). "Impact of Marine Chemical Ecology Research on the Discovery and Development of New Pharmaceuticals". *Marine Drugs.* **21** (3): 174. 10.3390/md21030174.

[7] R. Fu, Y. Sun, W. Sheng, and D. Liao. (2017). "Designing Multi-Targeted Agents: An Emerging Anticancer Drug Discovery Paradigm". *European Journal of Medicinal Chemistry.* **136** : 195-211. 10.1016/j.ejmech.2017.05.016.

[8] A. Narayanankutty, A. C. Famurewa, and E. Oprea. (2024). "Natural Bioactive

Compounds and Human Health". *Molecules.* **29** (14): 3372. 10.3390/molecules29143372.

[9] N. Bano, S. Parveen, M. Saeed, S. Siddiqui, M. Abohassan, and S. S. Mir. (2024). "Drug Repurposing of Selected Antibiotics: An Emerging Approach in Cancer Drug Discovery". *ACS Omega.* **9** (25): 26762-26779. 10.1021/acsomega.4c00617.

[10] C. Pfab, L. Schnobrich, S. Eldnasoury, A. Gessner, and N. El-Najjar. (2021). "Repurposing of Antimicrobial Agents for Cancer Therapy: What Do We Know?". *Cancers.* **13** (13): 3193. 10.3390/cancers13133193.

[11] L. Fang, L. Xu, M. Kader, T. Ding, S. Lu, D. Wang, A. R. Sharma, and Z. Zhang. (2025). "Salt-Adapted Microorganisms: A Promising Resource for Novel Anti-Cancer Drug Discovery". *Marine Drugs.* **23** (8): 296. 10.3390/md23080296.

[12] A. J. Rathinam, H. Santhaseelan, H. U. Dahms, V. T. Dinakaran, and S. G. Murugaiah. (2023). "Bioprospecting of Unexplored Halophilic Actinobacteria Against Human Infectious Pathogens". *3 Biotech.* **13** (12): 398. 10.1007/s13205-023-03812-8.

[13] S. Z. Alshawwa, K. S. Alshallash, A. Ghareeb, A. M. Elazzazy, M. Sharaf, A. Alharthi, F. E. Abdelgawad, D. El-Hossary, M. Jaremko, A. Emwas, and Y. A. Helmy. (2022). "Assessment of Pharmacological Potential of Novel Exopolysaccharide Isolated from Marine Kocuria sp. Strain AG5: Broad-Spectrum Biological Investigations". *Life.* **12** (9): 1387. 10.3390/life12091387.

[14] J. Jia, X. Wang, J. Sang, Z. Li, S. Lin, Z. Deng, and T. Huang. (2023). "An N-N Linked Dimeric Indole Alkaloid from the Marine Sponge-Associated Rare Actinomycetes Kocuria sp. S42". *Natural Product Research.* **37** (21): 3647-3653. 10.1080/14786419.2022.2098496.

[15] P. Foti, C. Caggia, and F. V. Romeo. (2025). "New Insight into Microbial Exploitation to Produce Bioactive Molecules from Agrifood and By-Products' Fermentation". *Foods.* **14** (8). 10.3390/foods14081439.

[16] Z. Wang, D. Zeng, Y. Zhu, M. Zhou, A. Kondo, T. Hasunuma, and X. Zhao. (2025). "Fermentation Design and Process Optimization Strategy Based on Machine Learning". *BioDesign Research.* **7** (1): 100002. 10.1016/j.bidere.2025.100002.

[17] A. Setiawan, W. Widyastuti, A. Irawan, O. S. Wijaya, A. Laila, W. A. Setiawan, N. L. G. R. Juliasih, K. Nonaka, M. Arai, and J. Hendri. (2021). "Solid State Fermentation of Shrimp Shell Waste Using Pseudonocardia carboxydivorans 18A13O1 to Produce Bioactive Metabolites". *Fermentation.* **7** (4): 247. 10.3390/fermentation7040247.

[18] X. Yang, L. Yuan, M. Zeeshan, C. Yang, W. Gao, G. Zhang, and C. Wang. (2025). "Optimization of Fermentation Conditions to Increase the Production of Antifungal Metabolites from Streptomyces sp. KN37". *Microbial Cell Factories.* **24** (1): 26. 10.1186/s12934-025-02652-w.

[19] M. Suliman, A. S. Bishr, S. T. K. Tohamy, M. Y. Alshahrani, and K. M. Aboshanab. (2025). "Solid-State Fermentation of Pristinamycin by Streptomyces pristinaespiralis NRRL ISP-5338 Using D-Optimal Design". *Bioprocess and Biosystems Engineering.* **48** (9): 1467-1479. 10.1007/s00449-025-03188-4.

[20] X. Ma, G. Gözaydın, H. Yang, W. Ning, X. Han, N. Y. Poon, H. Liang, N. Yan, and K. Zhou. (2020). "Upcycling Chitin-Containing Waste into Organonitrogen Chemicals via an Integrated Process". *Proceedings of the National Academy of Sciences of the United States of America.* **117** (14): 7719-7728. 10.1073/pnas.1919862117.

[21] A. Setiawan, F. Setiawan, N. L. G. R. Juliasih, W. Widyastuti, A. Laila, W. A. Setiawan, F. M. Djailani, M. Mulyono, J. Hendri, and M. Arai. (2022). "Fungicide Activity of Culture Extract from Kocuria palustris 19C38A1 Against Fusarium oxysporum". *Journal of Fungi.* **8** (3): 280. 10.3390/jof8030280.

[22] R. Subramani and W. Aalbersberg. (2013). "Culturable Rare Actinomycetes: Diversity, Isolation and Marine Natural Product Discovery". *Applied Microbiology and*

Biotechnology. **97** (21): 9291-9321. 10.1007/s00253-013-5229-7.

[23] W. Widyastuti, F. Setiawan, C. A. Afandy, A. Irawan, A. Laila, N. L. G. R. Juliasih, W. A. Setiawan, M. Arai, J. Hendri, and A. Setiawan. (2022). "Antifungal Agent Chitooligosaccharides Derived from Solid-State Fermentation of Shrimp Shell Waste by Pseudonocardia antitumoralis 18D36-A1". *Fermentation.* **8** (8): 353. 10.3390/fermentation8080353.

[24] A. Setiawan, F. Setiawan, S. Susianti, W. A. Setiawan, P. Ahmadi, R. Pangestu, J. Hendri, and N. L. G. R. Juliasih. (2025). "Chemical Profile of The Ethyl Acetate Extract of Aspergillus sydowi 22-PLP1-F1 as Antibacterial Agent Against Clinically Resistant Strains of Staphylococcus aureus and Pseudomonas aeruginosa". *Journal of Multidisciplinary Applied Natural Science.* **5** (1). 10.47352/jmans.2774-3047.238.

[25] A. Setiawan, R. Lutfiah, N. L. G. R. Juliasih, W. A. Setiawan, J. Hendri, and M. Arai. (2022). "Antibacterial Activity of EtOAc Extract from Marine-Derived Fungus Aspergillus nomiae A12-RF Against Clinical Pathogen Bacteria, Staphylococcus aureus". *AACL Bioflux.* **15** (3): 1413-1421.

[26] P. Ahmadi, M. Higashi, N. J. D. Voogd, and J. Tanaka. (2017). "Two Furanosesterterpenoids from the Sponge Luffariella variabilis". *Marine Drugs.* **15** (8): 249. 10.3390/md15080249.

[27] R. Schmid, S. Heuckeroth, A. Korf, A. Smirnov, O. Myers, T. S. Dyrlund, R. Bushuiev, K. J. Murray, N. Hoffmann, M. Lu, A. Sarvepalli, Z. Zhang, M. Fleischauer, K. Dührkop, M. Wesner, S. J. Hoogstra, E. Rudt, O. Mokshyna, and C. Brungs. (2023). "Integrative Analysis of Multimodal Mass Spectrometry Data in MZmine 3". *Nature Biotechnology.* **41** (4): 447-449. 10.1038/s41587-023-01690-2.

[28] A. Daina, O. Michielin, and V. Zoete. (2017). "SwissADME: A Free Web Tool to Evaluate Pharmacokinetics, Drug-Likeness and Medicinal Chemistry Friendliness of Small Molecules". *Scientific Reports.* **7** (1): 42717. 10.1038/srep42717.

[29] A. Daina and V. Zoete. (2024). "Testing the Predictive Power of Reverse Screening to Infer Drug Targets, with the Help of Machine Learning". *Communications Chemistry.* **7** (1): 105. 10.1038/s42004-024-01179-2.

[30] E. F. Pettersen, T. D. Goddard, C. C. Huang, G. S. Couch, D. M. Greenblatt, E. C. Meng, and T. E. Ferrin. (2004). "UCSF Chimera: A Visualization System for Exploratory Research and Analysis". *Journal of Computational Chemistry.* **25** (13): 1605-1612. 10.1002/jcc.20084.

[31] I. V. Ferrari and P. Patrizio. (2021). "Development and Validation Molecular Docking Analysis of Human Serum Albumin (HSA)". *bioRxiv*. 10.1101/2021.07.09.451789.

[32] J. Fuhrmann, A. Rurainski, H. P. Lenhof, and D. Neumann. (2010). "A New Lamarckian Genetic Algorithm for Flexible Ligand-Receptor Docking". *Journal of Computational Chemistry.* **31** (9): 1911-1918. 10.1002/jcc.21478.

[33] N. K. Subramani and S. Venugopal. (2024). "Molecular Docking and Dynamic Simulation Studies of Bioactive Compounds from Traditional Medicinal Compounds Against Exfoliative Toxin B from Staphylococcus aureus". *Journal of Pharmacology and Pharmacotherapeutics.* **15** (3): 316-326. 10.1177/0976500X241266072.

[34] A. van der Meij, H. Tyrrell, D. J. Sokolowski, E. M. F. Shepherdson, M. A. Elliot, and J. R. Nodwell. (2025). "Streptomyces venezuelae Uses Secreted Chitinases and a Designated ABC Transporter to Support the Competitive Saprophytic Catabolism of Chitin". *PLOS Biology.* **23** (8): e3003292. 10.1371/journal.pbio.3003292.

[35] X. Sun, Y. Zhao, and G. Ding. (2023). "Morphogenesis and Metabolomics Reveal the Compatible Relationship Among Suillus bovinus, Phialocephala fortinii, and Their Co -Host, Pinus massoniana". *Microbiology Spectrum.* **11** (5): e01453-23. 10.1128/spectrum.01453-23.

[36] C. Chakansin, J. Yostaworakul, C. Warin, K.

Kulthong, and S. Boonrungsiman. (2022). "Resazurin Rapid Screening for Antibacterial Activities of Organic and Inorganic Nanoparticles: Potential, Limitations and Precautions". *Analytical Biochemistry.* **637** : 114449. 10.1016/j.ab.2021.114449.

[37] A. M. Mayer, M. L. Pierce, K. Howe, A. D. Rodríguez, O. Taglialatela-Scafati, F. Nakamura, and N. Fusetani. (2022). "Marine Pharmacology in 2018: Marine Compounds with Antibacterial, Antidiabetic, Antifungal, Anti-Inflammatory, Antiprotozoal, Antituberculosis and Antiviral Activities; Affecting the Immune and Nervous Systems, and Other Miscellaneous Mechanisms of Action". *Pharmacological Research.* **183** : 106391. 10.1016/j.phrs.2022.106391.

[38] A. T. Dharmaraja. (2017). "Role of Reactive Oxygen Species (ROS) in Therapeutics and Drug Resistance in Cancer and Bacteria". *Journal of Medicinal Chemistry.* **60** (8): 3221 -3240. 10.1021/acs.jmedchem.6b01243.

[39] A. González, D. Vázquez, and A. Jiménez. (1979). "Inhibition of Translation in Bacterial and Eukaryotic Systems by the Antibiotic Anthelmycin (Hikizimycin)". *Biochimica et Biophysica Acta - Nucleic Acids and Protein Synthesis.* **561** (2): 403-409. 10.1016/0005-2787(79)90148-5.

[40] A. Hirata, M. Sumiyoshi, H. Fujita, M. Akimoto, M. H. R. A. Padayao, Y. Eguchi, M. Matsuura, M. Otsuka, K. Inada, A. Teshima, and K. Arakawa. (2025). "Rare Distribution of Butenolide-Type Signaling Molecules Among Streptomyces Strains and Functional Importance as Inducing Factors for Secondary Metabolite Production in Streptomyces rochei 7434AN4". *The Journal of Antibiotics.* **78** (8): 488-499. 10.1038/s41429-025-00840-9.

[41] Y. Hongo, T. Nakamura, S. Takahashi, T. Motoyama, T. Hayashi, H. Hirota, H. Osada, and H. Koshino. (2014). "Detection of Oxygen Addition Peaks for Terpendole E and Related Indole-Diterpene Alkaloids in a Positive-Mode ESI-MS". *Journal of Mass Spectrometry.* **49** (6): 537-542. 10.1002/jms.3360.

[42] S. Rai, L. S. Singh, K. Liriina, K. Jeyaram, T. Parija, and D. Sahoo. (2025). "Novel Endophytic Actinomycetes Species Streptomyces panacea of Panax sokpayensis Produce Antimicrobial Compounds Against Multidrug Resistant Staphylococcus aureus". *Scientific Reports.* **15** (1): 19863. 10.1038/s41598-025-05333-1.

[43] F. A. M. Gomaa, H. M. R. M. Selim, M. Y. Alshahrani, and K. M. Aboshanab. (2024). "Central Composite Design for Optimizing Istamycin Production by Streptomyces tenjimariensis". *World Journal of Microbiology and Biotechnology.* **40** (10): 316. 10.1007/s11274-024-04118-4.

[44] S. Demisie, D. Oh, A. Abera, G. Tasew, G. D. Satessa, F. Fufa, A. M. Shenkutie, D. Wolday, and K. Tafess. (2024). "Bioprospecting Secondary Metabolites with Antimicrobial Properties from Soil Bacteria in High-Temperature Ecosystems". *Microbial Cell Factories.* **23** (1): 332. 10.1186/s12934-024-02589-6.

[45] Y. Hou, M. Chen, Z. Sun, G. Ma, D. Chen, H. Wu, J. Yang, Y. Li, and X. Xu. (2022). "The Biosynthesis Related Enzyme, Structure Diversity and Bioactivity Abundance of Indole-Diterpenes: A Review". *Molecules.* **27** (20): 6870. 10.3390/molecules27206870.

[46] C. A. Lipinski. (2016). "Rule of Five in 2015 and Beyond: Target and Ligand Structural Limitations, Ligand Chemistry Structure and Drug Discovery Project Decisions". *Advanced Drug Delivery Reviews.* **101** : 34-41. 10.1016/j.addr.2016.04.029.

[47] S. P. Sweety, T. A. Rupok, S. A. Shoily, S. Parvin, J. Barmon, and M. E. Islam. (2025). "GC-MS Analysis, Molecular Docking and Pharmacokinetic Evaluation of Phytocompounds from Lagerstroemia speciosa (L.) Pers. Bark and Their Effect on Inflammation Target Proteins". *Food Chemistry Advances.* **9** : 101172. 10.1016/j.focha.2025.101172.

[48] D. Garcia Jimenez, V. Poongavanam, and J. Kihlberg. (2023). "Macrocycles in Drug Discovery—Learning from the Past for the Future". *Journal of Medicinal Chemistry.* **66** (8): 5377-5396. 10.1021/acs.jmedchem.3c00134.

[49] F. Susa, S. Arpicco, C. F. Pirri, and T. Limongi. (2024). "An Overview on the Physiopathology of the Blood-Brain Barrier and the Lipid-Based Nanocarriers for Central Nervous System Delivery". *Pharmaceutics.* **16** (7): 849. 10.3390/pharmaceutics16070849.

[50] A. Talevi and C. L. Bellera. (2022). In: "The ADME Encyclopedia". Cham: Springer Nature Switzerland. 10.1007/978-3-030-84860-6_73.

[51] S. Kalyaanamoorthy, S. M. Lamothe, X. Hou, T. C. Moon, H. T. Kurata, M. Houghton, and K. H. Barakat. (2020). "A Structure-Based Computational Workflow to Predict Liability and Binding Modes of Small Molecules to hERG". *Scientific Reports.* **10** (1): 16262. 10.1038/s41598-020-72889-5.

[52] A. Claesson and A. Minidis. (2018). "Systematic Approach to Organizing Structural Alerts for Reactive Metabolite Formation from Potential Drugs". *Chemical Research in Toxicology.* **31** (6): 389-411. 10.1021/acs.chemrestox.8b00046.

[53] K. C. Baral and K. Y. Choi. (2025). "Barriers and Strategies for Oral Peptide and Protein Therapeutics Delivery: Update on Clinical Advances". *Pharmaceutics.* **17** (4): 397. 10.3390/pharmaceutics17040397.

[54] S. A. Putri, R. Maharani, I. P. Maksum, and T. J. Siahaan. (2025). "Peptide Design for Enhanced Anti-Melanogenesis: Optimizing Molecular Weight, Polarity, and Cyclization". *Drug Design, Development and Therapy.* **19** : 645-670. 10.2147/DDDT.S500004.

[55] L. Ali and M. H. Abdel Aziz. (2024). "Crosstalk Involving Two-Component Systems in Staphylococcus aureus Signaling Networks". *Journal of Bacteriology.* **206** (4): e00418-23. 10.1128/jb.00418-23.

[56] M. Wang, C. Fang, B. Ma, X. Luo, and Z. Hou. (2020). "Regulation of Cytokinesis: FtsZ and Its Accessory Proteins". *Current Genetics.* **66** (1): 43-49. 10.1007/s00294-019-01005-6.

[57] S. C. Gupta, S. Prasad, J. H. Kim, S. Patchva, L. J. Webb, I. K. Priyadarsini, and B. B. Aggarwal. (2011). "Multitargeting by Curcumin as Revealed by Molecular Interaction Studies". *Natural Product Reports.* **28** (12): 1937-1955. 10.1039/C1NP00051A.

[58] Y. Zheng, R. Du, S. Cai, Z. Liu, Z. Fang, T. Liu, L. So, Y. Lu, N. Sun, and K. Wong. (2018). "Study of Benzofuroquinolinium Derivatives as a New Class of Potent Antibacterial Agent and the Mode of Inhibition Targeting FtsZ". *Frontiers in Microbiology.* **9** : 1937. 10.3389/fmicb.2018.01937.

[59] J. M. Barrows and E. D. Goley. (2021). "FtsZ Dynamics in Bacterial Division: What, How, and Why?". *Current Opinion in Cell Biology.* **68** : 163-172. 10.1016/j.ceb.2020.10.013.

[60] A. M. Tovar-Nieto, L. E. Flores-Padilla, B. Rivas-Santiago, J. V. Trujillo-Paez, E. E. Lara-Ramirez, Y. M. Jacobo-Delgado, J. E. López-Ramos, and A. Rodríguez-Carlos. (2024). "The Repurposing of FDA-Approved Drugs as FtsZ Inhibitors Against Mycobacterium tuberculosis: An In Silico and In Vitro Study". *Microorganisms.* **12** (8): 1505. 10.3390/microorganisms12081505.

[61] K. Shi, G. Wang, J. Pei, J. Zhang, J. Wang, L. Ouyang, Y. Wang, and W. Li. (2022). "Emerging Strategies to Overcome Resistance to Third-Generation EGFR Inhibitors". *Journal of Hematology and Oncology.* **15** (1): 94. 10.1186/s13045-022-01311-6.

[62] L. Saldaña-Rivera, M. Bello, and D. Méndez-Luna. (2019). "Structural Insight into the Binding Mechanism of ATP to EGFR and L858R, and T790M and L858R/T790 Mutants". *Journal of Biomolecular Structure and Dynamics.* **37** (17): 4671-4684. 10.1080/07391102.2018.1558112.

[63] M. L. Uribe, I. Marrocco, and Y. Yarden. (2021). "EGFR in Cancer: Signaling Mechanisms, Drugs, and Acquired Resistance". *Cancers.* **13** (11): 2748. 10.3390/cancers13112748.

[64] P. N. Sonwane and M. R. Kumbhare. (2025). "Molecular Docking and Pharmacokinetics of Benzimidazole-Based FtsZ Inhibitors for Tuberculosis". *Scientific Reports.* **15** (1): 35270. 10.1038/s41598-025-18084-w.

[65] M. S. R, Y. H. S, S. M. A. Sangi, A. K. N, S. Shaik, S. Nagaraja, G. Meravanige, M. M. Islam, P. K. Sreenivasalu, R. M. Almuqbil, S. Chohan, B. Pandey, S. Thapa, and A. V. Atoki. (2026). "In Silico Screening of Marine Fungal Metabolites Identifies Potential FtsZ Inhibitors Against MDR-Tuberculosis Through Docking and Molecular Dynamics Analysis". *Scientific Reports.* **16** (1): 4030. 10.1038/s41598-025-34116-x.

[66] M. Fan, L. Hu, S. Shi, X. Song, H. He, and B. Qi. (2023). "Design, Synthesis and Biological Evaluation of EGFR Kinase Inhibitors That Span the Orthosteric and Allosteric Sites". *Bioorganic and Medicinal Chemistry.* **96** : 117534. 10.1016/j.bmc.2023.117534.